

# Proof-of-Concept and Advancement of the CellFlux Concept

Christian Odenthal and Wolf-Dieter Steinmann <sup>a)</sup>

*German Aerospace Center (DLR), Institute of Technical Thermodynamics  
Paffenwaldring 38-40, 70569 Stuttgart*

<sup>a)</sup> Corresponding author: wolf.steinmann@dlr.de

**Abstract.** The CellFlux storage system is a new concept for reducing the costs of medium to high temperature thermal energy storage. Initially designed for solar thermal power plants, the concept is suitable for industrial processes and power to heat applications as well. This paper gives first results of a new pilot scale plant set up at DLR in Stuttgart as a proof of concept. Experimental results are used for the validation of a simplified model. The model is applied to calculate pareto optimal storage configurations in terms of necessary storage mass and exergetic efficiency, suitable for two types of solar thermal power plants. Particularly for applications having larger temperature differences, high exergetic efficiencies at low costs for the storage material can be achieved.

## INTRODUCTION

The CellFlux concept has been developed as an alternative solution for sensible heat storage [1]. The storage system consists of a regenerator type storage volume and a finned tube heat exchanger. Heat is transferred from a primary heat transferring fluid (HTF) to a gaseous intermediate working fluid (IWF) which then transfers the heat in direct contact to the storage volume. The IWF is kept in an enclosed loop and conveyed by a fan. While one focus of this development is on reducing costs, another characteristic of the CellFlux approach is high versatility. Cost reduction is accomplished by using a packed bed of low cost solid storage materials. Air at ambient pressure is applied as an IWF, CO<sub>2</sub> or steam are some other options. Solid storage materials allow a wide operation temperature range; another advantage is the avoidance of risks resulting from solidification, leakage or flammability. With its unique approach, CellFlux allows for low cost storage in a packed bed for a multitude of HTFs. A further element of the concept is modularity. Many storage cells are combined to build a storage system. This allows shortening the total length of the air flow path compared to a single large unit. The standardization of storage cells results in cost reductions. Depending on the number of cells, the power and capacity of the storage system can be varied over a wide range. This facilitates the application of CellFlux storage units not only for CSP plants but also for small and medium scale process heat applications at comparable specific costs.

## EXPERIMENTAL SETUP

As a proof of concept, a large scale experimental plant has been set up at DLR in Stuttgart. The plant is designed to investigate the transient behavior of the CellFlux concept for thermal oil based CSP power plants. Hence, the upper temperature of the plant is limited to 390°C. The following section gives an overview of the plant and details about the investigated materials.

### Overview of the Plant

Figure 1 shows a 3D drawing of the complete plant and a picture of the regenerator storage volume on the outside. For the regenerator, a new concept is applied with a horizontal flow direction. It is based on a 40 ft ISO-container, which is insulated on the inside with 350 mm thick insulation. A fan is used to convey the air, followed by a switching valve arrangement to divert the air to either the storage volume or the heat exchanger. During

charging, the air enters the finned tube heat exchanger first, where it is heated by a liquid HTF (Syltherm 800) and then flows to the regenerator storage. Here, heat is transferred to the storage material, causing the air to cool down to the lower temperature. The air then returns to the fan through the long duct seen on both pictures. Midway, a thermal mass flow meter is used to measure the air mass flow. During discharge, the air is diverted directly into the regenerator, where it is heated. The hot air leaves the regenerator and flows through the heat exchanger, where the thermal energy is transferred back to the primary working fluid.

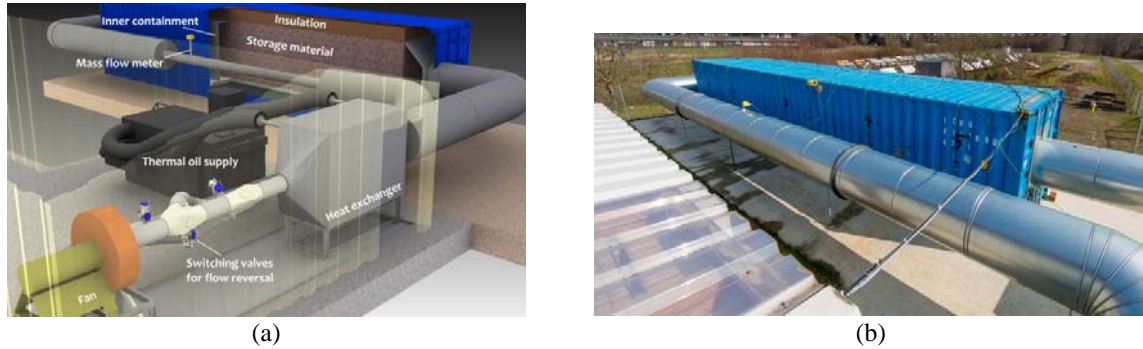


**FIGURE 1.** (a) Inventor drawing of the plant, (b) picture of the regenerator storage volume on the outside.

On the inside of the ISO-container is an air tight inner containment, which is filled with the storage material. A sketch is shown in Figure 2. The packing is divided into eleven sections, numbered from zero to ten. Each section has a length of one meter. The temperature is measured along the middle axis in the flow direction at each plane. In this work, temperatures at plane zero and ten are taken. Furthermore, by a 3x3 pattern of thermocouples in plane 0, 2, 5, 8 and 10 the radial temperature distribution can be measured. Each section is equipped with three static pressure probes, allowing for the measurement of pressure differences between arbitrary sections. Hence, pressure drop can be measured over short distances as well as over the whole bed. The insulation is equipped with additional thermocouple pairs to measure heat losses through the regenerator walls. The additional sections at the ends of the packing are 600 mm in length and filled with ceramic saddles for flow stratification.

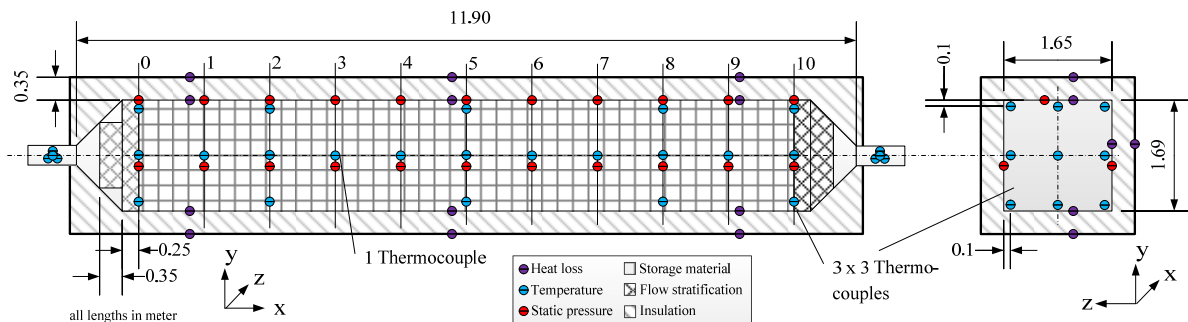


**FIGURE 2.** Sketch of the regenerator storage volume and position of thermocouples and pressure probes inside the pilot scale storage volume

Bricks with a total volume of 30 m<sup>3</sup> are used as the storage material. A thermal oil loop is used to heat the air to 380 °C. Depending on the cyclic temperature difference, up to 2500 kWh<sub>th</sub> can be stored; the power is approximately 100 kW during discharging. For measuring the mass flow, a thermal mass flow meter is used. Albeit the accuracy is 0.75 % ±0.00595 kg/s, there arises further uncertainty of 2 % by possible moisture in the intermediate working fluid loop and variations in the duct diameter. For the thermocouples, the absolute accuracy lies in the range of ±2 Kelvin, however, preliminary tests have shown that the relative error between neighboring thermocouples is less than 0.5 Kelvin.

## Geometric Properties of the Storage Material

The storage material is modeled as channel flow. Due to the irregular shape of the flow channels, simplified expressions must be found for the coring bricks. Figure 3 illustrates the proportions of the brick material. A flow channel having a free flow area  $A_{0,g}$  is surrounded by a solid mass with the cross sectional area  $A_{0,s}$ . The porosity is derived from the ratio of the free flow area and total cross sectional area:

$$\varepsilon = \frac{A_{0,g}}{A_{0,s} + A_{0,g}}. \quad (1)$$

The hydraulic diameter  $d_{\text{hyd}}$  is calculated from the free flow area  $A_{0,g}$  and the circumference  $U$  of the flow channel. Different flow channel diameters are averaged out:

$$d_{\text{hyd}} = \frac{4A_{0,g}}{U} = 4 \sum_i^n \frac{A_{i,0,g}}{U_i}. \quad (2)$$

The effective conduction length  $L_s$  is defined as the length that has to be multiplied by the circumference to yield the cross sectional area of the solid material [2]:

$$L_s = \frac{A_{0,s}}{U} = \frac{A_{0,s}}{a_v(A_{0,s} + A_{0,g})} = \frac{(1 - \varepsilon)}{a_v} = \frac{(1 - \varepsilon) \cdot d_{\text{hyd}}}{4\varepsilon}. \quad (3)$$

The properties of the pilot plant and the storage material are summarized in the following table.

**TABLE 1.** Summary of plant and storage material properties

porosity $\varepsilon$	35.58	%
hydraulic diameter $d_{\text{hyd}}$	13.75	mm
density of the storage material	2313	kg/m <sup>3</sup>
number of brick rows	84	-
total mass	39799	kg
surface roughness $K$ (smooth concrete)	0.3	mm

## NUMERIC MODEL

To perform a numerous sizing calculations, a fast model is necessary, which is described in the next section. The focus for the model validation lies on the storage volume, thus, a model of the heat exchanger is omitted.

### Mathematical Formulation

Fast calculation is achieved by applying a simplified one dimensional model. Hence, only two coupled differential equations in each node are necessary. The model assumes several simplifications:

- No intraparticle heat diffusion, since convection dominates when no stand-by operation is considered
- Uniform temperature of the storage material within each node
- Heat capacity of the gaseous phase is small compared to the solid and therefore neglected
- No heat loss to the environment

For the gaseous phase, equation (4) expresses the differential equation for the gas phase:

$$0 = -\rho_g c_{p,g} v_{0,x,g} \frac{\partial T_g}{\partial x} + \dot{Q}_g''' \quad (4)$$

The differential equation for the solid phase is expressed by

$$(1 - \varepsilon) \rho_s c_{p,s} \frac{\partial T_s}{\partial t} = \dot{Q}_s''' \quad (5)$$

Both equations are coupled by a volumetric source term, where  $k_{\text{vol}}$  denotes the heat transfer coefficient:

$$\dot{Q}_g''' = -\dot{Q}_s''' = k_{\text{vol}} \cdot (T_s - T_g). \quad (6)$$

If the thickness of the storage material is large, additional resistance due to conduction must be considered as well. According to Sragovic [3], this is the case if the Biot number is smaller than 0.1. Hausen [4] derived simplified coefficients for various geometries.  $h_{\text{vol}}$  denotes the volumetric heat transfer coefficient,  $\lambda_s$  the conductivity of the solid and  $L_s$  is the effective conduction length.

$$k_{\text{vol}} = \frac{1}{h_{\text{vol}}} + \frac{\lambda_s}{C \cdot L_s}, \quad \text{with } C = \begin{cases} 3 & \text{for plates} \\ C_{\text{cyl}} & \text{for hollow cylinders} \\ 5 & \text{for spheres} \end{cases} \quad (7)$$

The coefficient for the hollow cylinder was derived by [5]. Herby  $r_a$  and  $r_i$  are the outer and inner diameter of the hollow cylinder and  $d_{\text{hyd}}$  is the hydraulic diameter.

$$C_{\text{cyl}} = \frac{L_s}{r_i \cdot \frac{r_a^4}{(r_a^2 - r_i^2)^2} \cdot \ln\left(\frac{r_a}{r_i}\right) - 2r_a^2 + r_i^2}, \quad \text{with } r_i = \frac{d_{\text{hyd}}}{2}, r_a = r_i + L_s \quad (8)$$

Pressure losses are calculated from a general loss equation, where the overall loss coefficient  $\zeta_{\text{tot}}$  is derived from pressure loss measurements:

$$\Delta p = \zeta_{\text{tot}} \frac{\rho_g}{2} v_g^2. \quad (9)$$

The differential equations are spatially discretized by an upwind scheme of the first order. The time-wise discretization is fully implicit. After nondimensionalization, equation (4) now reads

$$\frac{\theta_{g,i}^{n+1} - \theta_{g,i}^n}{\Delta \xi} = \Lambda \cdot (\theta_{s,i}^{n+1} - \theta_{g,i}^{n+1}). \quad (10)$$

For the solid phase, equation (5) becomes

$$\frac{\theta_{s,i}^{n+1} - \theta_{s,i}^n}{\Delta \tau} = \Pi \cdot (\theta_{g,i}^{n+1} - \theta_{s,i}^{n+1}). \quad (11)$$

Hereby, the following nondimensional coefficients occur.  $L_{\text{Reg}}$  denotes the flow length of the regenerator,  $t_{\text{ref}}$  a reference time and  $T_{\text{ref}}$  the reference temperature for nondimensionalization.  $\dot{m}_g$  is the mass flow of the gas,  $c_{p,g}$  the heat capacity,  $V_{\text{Reg}}$  the volume of the regenerator,  $\rho_s$  the density of the solid material,  $c_s$  the specific heat capacity and  $\varepsilon$  the porosity of the regenerator packing.

$$\Lambda = \frac{V_{\text{Reg}} \cdot k_{\text{vol},f-s}}{\dot{m}_g c_{p,g}}, \quad \Pi = \frac{t_{\text{ref}} \cdot k_{\text{vol},f-s}}{\rho_s c_s (1 - \varepsilon)}, \quad \theta = \frac{T}{T_{\text{ref}}}, \quad \tau = \frac{t}{t_{\text{ref}}}, \quad \xi = \frac{x}{L_{\text{Reg}}} \quad (12)$$

The discretization scheme for the model is shown in Figure 3b.

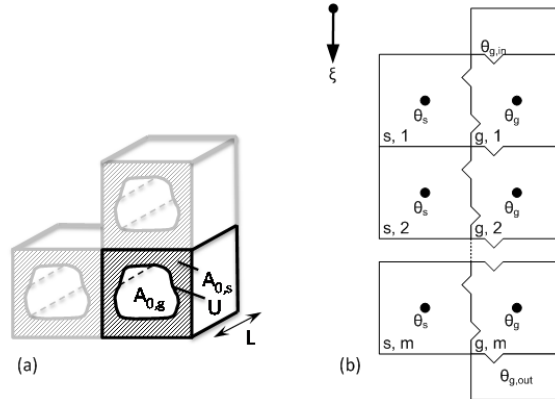


FIGURE 3. Proportions of the coring brick material (a) and discretization scheme (b)

The temperature-dependent thermodynamic properties of the gas and the storage material are calculated from the known temperature values of the preceding time step (*Backward-Time-Approximation*). This assumption is justified, since temperature gradients are small between each time step. The time-wise discretization yields a system of linear equations with a sparse band matrix  $\bar{M}$ , with  $\theta^{n+1}$  denoting the vector of the temperature field at the new time step  $n + 1$  and  $\theta^n$  at the preceding time step  $n$ . The boundary conditions are represented by the vector  $b$ .

$$\bar{M} \cdot \theta^{n+1} = \theta^n + b \quad (13)$$

The equations are implemented in Matlab® and solved at each time step by left-handed multiplication of the inverse  $\bar{M}^{-1}$ .

## Model Validation

For model validation, the measured mass flow and inlet temperature are fed into the model. Temperatures are taken from the first plane at the beginning and the last plane at the end of the packing material. The model is discretized with 120 nodes and a time step of 15 seconds. Figure 4 shows the measured temperatures inside the regenerator at different times in comparison with the computed temperature distribution. As can be seen, there is a good agreement with the shape of the temperature distributions, meaning that the heat transfer is modeled correctly. However, it can be seen as well that the curves are shifted over the course of time. The reason for that is either an incorrect heat capacity of the storage material or an error in the mass flow measurement. In preliminary tests, the change in inner energy was compared with cumulated energy from the enthalpy streams and heat losses. Since these results are in good agreement and thermodynamic properties of the material have been carefully measured in lab scale experiments, deviations in the actual mass flow along the middle axis are more likely. Hence, computations have been conducted with the actual mass flow and with a value increased by 20 %. For the case with increased mass flow, the model fits very well to the experimental results. Therefore, it must be assumed that inside the storage volume a slight flow maldistribution occurs where slightly more than the average mass flow streams along the middle axis.

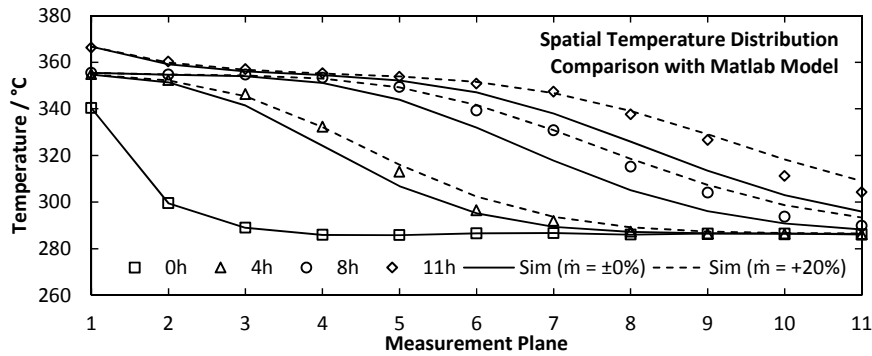


**FIGURE 4.** Comparison of measured spatial temperature distribution inside the regenerator with simplified Matlab model

## SYSTEM ANALYSIS

The model described in the preceding section is used for a system analysis of the CellFlux concept in combination with a parabolic trough solar thermal power plant.

### Methodology

A regenerator type storage volume is always in a transient condition during charging and discharging. In order to optimize the operation strategy of the CellFlux concept, system analysis is done by the application of simulation tools on various levels. The analysis of a single storage cell helps to identify the optimal combination of heat exchanger and storage volume and also allows determination of the best geometry of the storage volume for a given storage material. Two different solar thermal power plant technologies are compared. The first represents the state of

the art, thermal oil (VP1) based power plant. The second is an alternative based on molten salt as HTF (Hitec HTS). From both technologies, boundary conditions are derived for the rating of the storage configurations. The logarithmic temperature difference in the heat exchanger is fixed to 15 Kelvin. Air is used as the intermediate working fluid. The following parameters are varied in an extensive parametric study:

- Maximum permitted change of the exit temperature ( $\Delta T_e$ )
- Hydraulic diameter ( $d_{\text{hyd}}$ )
- Porosity ( $\varepsilon$ )
- Free flow cross-sectional area of the regenerator ( $A_0$ )

Simultaneously, the flow length of the regenerator is adjusted in a way that exactly 8 hours storage time at cyclic quasi-stationary operation is met. For this, the Matlab model is coupled with a minimization routine, based on a simplex algorithm. Table 2 summarizes the input parameters for the parametric study.

**TABLE 2.** Input parameters for the parametric study

	VP1	Hitec HTS	
thermal power per module	10	20	MW
number of modules	14	14	-
nominal inlet temperature HTF	390	510	
charging temperature IWF	375	495	°C
maximum temperature difference	100	200	K
mass flow IWF	94,8	93,5	kg/s
electric efficiency of the fans		80	%
maximum permitted exit temperature ( $\Delta T_e$ )		10 - 90	%
free flow area of the regenerator ( $A_0$ )		100 - 600	m <sup>2</sup>
hydraulic diameter ( $d_{\text{hyd}}$ )		10 - 150	mm
Porosity ( $\varepsilon$ )		20 - 50	%

In a preceding publication [6], the impact of steel mass and parasitic losses of the heat exchanger on investment and operational costs were presented. Similar to that, the necessary material mass of the regenerator packing together with the recovered exergy from the storage system are two meaningful quantities for the estimation of operational and investment costs.

To quantify exergetic efficiency of a CellFlux storage system, an exergetic efficiency  $\mathcal{E}$ , often referred to as the rational exergetic efficiency, is used here. It is defined as the exergy regained during discharge from the storage system  $\Delta E''_{\text{sto}}$ , where the exergy destruction of the fan to overcome the pressure drop inside the regenerator  $\Delta E_{\text{reg,fan}}$  is subtracted. This exergy is divided by the available exergy from the solar field  $\Delta E_{a,0}'$  during eight hours of charging process. Additionally, exergetic losses caused by the heat exchanger must be taken into account as well. These are the exergy destruction caused by pressure drop on the IWF side  $\Delta E_{\text{he,fan}}$  and the HTF side  $\Delta E_{\text{he,pump}}$ , both based also on the initially available exergy  $\Delta E_{a,0}'$ .

$$\mathcal{E} = \mathcal{E}_{\text{reg}} + \mathcal{E}_{\text{he}} = \frac{\Delta E''_{\text{sto}} - \Delta E_{\text{reg,fan}}}{\Delta E_{a,0}'} - \frac{\Delta E_{\text{he,fan}} + \Delta E_{\text{he,pump}}}{\Delta E_{a,0}'} \quad (14)$$

The initially available exergy is calculated from the exergy balance of the solar field at nominal conditions over the length of a full charging cycle  $t_e'$

$$\Delta E_{a,0}' = (\dot{E}'_{\text{out,nom}} - \dot{E}'_{\text{in,nom}}) \cdot t_e' \quad (15)$$

Exergy destruction due to parasitic losses occurs during charging and discharging, hence both periods must be considered.

$$\Delta E_{\text{reg,fan}} = \Delta E'_{\text{reg,fan}} + \Delta E''_{\text{reg,fan}} \quad (16)$$

The exergetic losses on the oil side occur inside the heat exchanger tubes and the pump. In case of the pump, the energy balance ( $1 \rightarrow 2$ ) is given by equation (17). Hereby,  $\dot{m}\bar{c}_f$  is the averaged heat capacity flow rate of the HTF,

$\Delta p$  the pressure change and  $\bar{\rho}$  the average density. With the electric energy consumption of the pump  $P_{el,pump}$  and its electric efficiency  $\eta_{el,pump}$ , the equation reads

$$P_{el,pump} \cdot \eta_{el,pump} = \dot{m}\bar{c}_f (\check{T}_2 - \check{T}_1) + \frac{\Delta p}{\bar{\rho}}. \quad (17)$$

For the heat exchanger, only the exergetic loss due to the flow is considered. Hence, heat transfer is neglected. The energy balance (2  $\rightarrow$  3) is

$$0 = \dot{m}\bar{c}_f (\check{T}_3 - \check{T}_2) - \frac{\Delta p}{\bar{\rho}}. \quad (18)$$

The entropy production between states (1  $\rightarrow$  3) is given by equation (19).

$$\dot{S}_{HTF,pump}^{irr} = \dot{m}\bar{c}_f \ln\left(\frac{\check{T}_3}{\check{T}_1}\right) = \dot{m}\bar{c}_f \ln\left(1 + \frac{P_{el,pump} \cdot \eta_{el,pump}}{\dot{m}\bar{c}_f \check{T}_1}\right). \quad (19)$$

Inserting the temperatures  $\check{T}_1$  and  $\check{T}_3$  from equations (17) and (18), the exergy destruction of the pump  $\Delta E_{he,pump}$  finally reads

$$\Delta E_{he,pump} = \check{T}_u \cdot \dot{S}_{HTF,pump}^{irr} = \check{T}_u \cdot \dot{m}\bar{c}_f \ln\left(1 + \frac{P_{el,pump} \cdot \eta_{el,pump}}{\dot{m}\bar{c}_f \check{T}_1}\right). \quad (20)$$

## Results

The parametric study yields various regenerator configurations. For each possible configuration, a specific exergetic efficiency  $\Xi_{reg}$  at the cost of a specific necessary storage material mass can be reached. Drawing this information in a diagram creates a scattered field of possible storage configurations. Fitting a curve along the lower end of the scattered data points represents a so-called pareto front. Any configuration above this line must be considered as inefficient, since there is a better configuration with the same exergetic efficiency but with less material needed. Any configuration below this line is technically not feasible.

The next figure shows pareto frontiers for both investigated power plant configurations. Since the cross-sectional area of the regenerator has a major influence on the design of the regenerator, pareto frontiers for different cross-sectional areas are drawn in a single diagram. From both diagrams, it can be seen that there is no need for cross-sectional areas larger than 400 m<sup>2</sup>, since pressure losses become very small behind this boundary.

Generally, there is a strong dependency between necessary storage mass of the regenerator and the exergetic efficiency. This dependency is almost linear until roughly 70 % efficiency is reached. Beyond this point, the necessary mass exponentially increases. The reason for this behavior is a complex interaction between all influencing parameters, mainly caused by the permissible change of the exit temperature. If the lowest amounts of necessary storage material mass should be achieved, the permissible change of the exit temperature must be as large as possible. Because of this, the regenerator is heated to almost uniform temperatures, causing the utilization to increase. A higher utilization results in less necessary material but also lowered exergetic efficiency. That is because towards the end of the charge and discharge cycles, the thermal power declines. If the permissible change of exit temperature is lowered, the curve follows the linear progression up to the point where 70 % efficiency is reached. At this point the utilization is much worse, needing significantly more storage material. Due to the increased flow length, pressure losses become more important as well. This must be compensated by a larger hydraulic diameter, lowering the heat transfer area and reducing the heat transfer. Hence, even more material is necessary, causing the onset of exponential progression. In the case of a perfect regenerator with no pressure losses, the maximum possible efficiency is shown in the upper right corners of the diagrams. The difference from 100 % arises from the logarithmic temperature difference in the CellFlux heat exchanger.

In a comparison of both power plants, there is a clear advantage for higher operating temperatures if higher temperature differences can be realized. In case of the Hitec HTS based power plant, the amount of stored energy in a single module can be doubled. Less necessary modules also mean less parasitic power consumption for driving fans and pumps. This effect can also be seen in the diagrams: the curves for the Hitec HTS based plant are slightly shifted to the right where exergetic efficiency is somewhat higher.

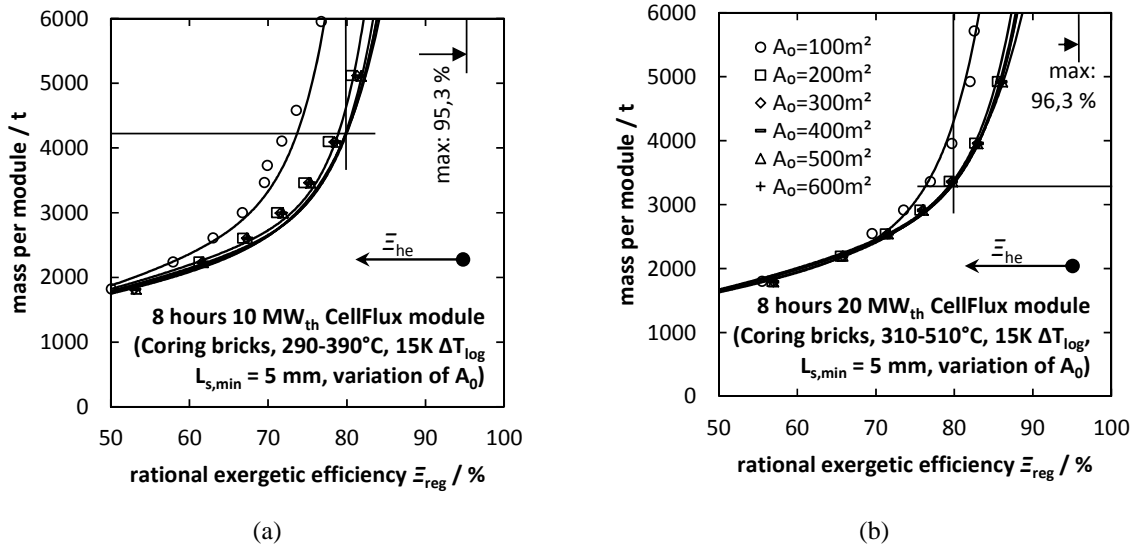


**FIGURE 5.** Necessary storage material mass for reaching a certain rational exergetic efficiency. (a) VP1 based power plant operating at 390 °C upper HTF temperature and (b) Hitec HTS based power plant with 510 °C upper HTF temperature

The system analysis shows that various possible configurations with different exergetic efficiencies of the CellFlux storage system can be designed. As an example, with 14 modules, a 50 MW<sub>el</sub>/140 MW<sub>th</sub> solar thermal power plant based on thermal oil could be supplied for 8 hours. If a rational exergetic efficiency of 80 % should be reached, 58800 tons of storage material are necessary. Assuming a material price of 100 €/ton, the price per kilowatt hour is 5.25 €/kWh<sub>th</sub>. The same number of modules would be necessary for a solar thermal power plant based on Hitec HTS with 125 MW<sub>el</sub>/280 MW<sub>th</sub>. With the same rational exergetic efficiency of 80 %, 46200 tons of storage material is necessary. However, the price per kilowatt hour drops down to 2.06 €/kWh<sub>th</sub>. In both cases, the rational exergetic efficiency must be reduced by the parasitic losses caused by the heat exchanger  $\epsilon_{he}$  (indicated by the arrow in the diagrams) and its costs must be added. The final assessment of a cost effective configuration must be done by an economic analysis. Here, the Hitec HTS based plant has an advantage, since the impact of parasitic losses is comparatively small due to the higher electric power. The relationships between exergetic efficiency and storage mass and the investigation of possible heat exchangers in a previous publication [6] provide a basis for such analyses. Considering the low costs for the storage material and some preliminary cost estimates, the overall costs of the CellFlux storage system are promising.

## REFERENCES

- [1] C. Odenthal, W.-D. Steinmann, M. Eck, and D. Laing, "The CellFlux Storage Concept for Cost Reduction in Parabolic Trough Solar Thermal Power Plants," *Energy Procedia*, vol. 46, pp. 142–151, 2014, DOI: 10.1016/j.egypro.2014.01.167.
- [2] W. Heiligenstädt, "Wärmetechnische Rechnungen für Industrieöfen," 1966.
- [3] D. Sragovich, "Transient analysis for designing and predicting operational performance of a high temperature sensible thermal energy storage system," *Sol. Energy*, vol. 43, no. 1, pp. 7–16, 1989, DOI: 10.1016/0038-092X(89)90095-9.
- [4] H. Hausen, *Wärmeübertragung im Gegenstrom, Gleichstrom und Kreuzstrom*, 2nd ed. Berlin, Germany: Springer Verlag, 1976.
- [5] F. W. Schmidt and A. J. Willmott, *Thermal energy storage and regeneration*, 1st ed. Washington, D.C., USA: Hemisphere Publishing Corporation, 1981.
- [6] C. Odenthal, W. Steinmann, and M. Eck, "The CellFlux Storage Concept for Increased Flexibility in Sensible Heat Storage," in *IREC 2015*, 2015.